# Molecularly Mediated Thin Film Assembly of Nanoparticles on Flexible Devices: Electrical Conductivity *versus* Device Strains in Different Gas/Vapor Environment

**Jun Yin, Peipei Hu, Jin Luo, Lingyan Wang, Melissa F. Cohen, and Chuan-Jian Zhong***

Department of Chemistry, State University of New York at Binghamton, Binghamton, New York 13902, United States

**ABSTRACT** The ability to precisely control nanoparticle-enabled electrical devices for applications involving conformal wrapping/bending adaptability in various complex sensing environments requires an understanding of the electrical correlation with the device strain and exposure to the molecular environment. This report describes novel findings of an investigation of molecularly mediated thin film assembly of gold nanoparticles on flexible chemiresistor devices under different device strains and exposure molecules. Both theoretical and experimental data have revealed that the electrical conductivity of the nanoparticle assembly depends on a combination of the device strain and the exposure molecules. Under no device strain, the electrical conductivity is sensitive to the molecular nature in the exposure environment, revealing a clear increase in electrical conductivity with the dielectric constant of vapor molecules. Under small device strains, the electrical conductivity is shown to respond sensitively to the strain directions (tensile *vs* compressive strain) and also to the dielectric constant of the vapor molecules in a way resembling the characteristic under no device strain. Under large device strains, the electrical conductivity is shown to respond to the difference in dielectric constant of the vapor molecules but, more significantly, to the device tensile and compressive strains than those under small device strains. This combination of device strain and dielectric characteristic is also dependent on the orientation of the microelectrode patterns with respect to the device strain direction, a finding that has important implications to the design of flexible arrays for a complex sensing environment.

**KEYWORDS:** molecularly engineered nanoparticles · thin film assembly flexible substrates · device strain · dielectric properties · chemical sensors

Metal or alloy nanoparticles have attracted increasing interests as chemical or biological sensing materials for various electrical devices such as chemiresistors and piezoelectric resonators on rigid substrates.[1−16] One example involves molecularly mediated thin film assemblies of gold or alloy nanoparticles *via* interparticle covalent bonding, hydrogen bonding, or van der Waals interaction[4−10] on microelectrode patterned glass substrates.[6−11,17−19] Recently, the study of functional devices on flexible substrates has become an important focal area of interest.[20−37] In comparison with conventional devices on rigid silicon, glass, or ceramic substrates, the attributes of flexible devices include simplified processing, low-cost manufacturing, and increased flexibility for their integration in wraps, lightweight electronics packaging platform, and conformal adaptability in various complex or special sensing environments. There has been an increasing number of reports on flexible substrates for chemical sensor devices,[21−38] a few of which explore nanoparticle thin film assemblies as sensing materials,[30−32] including our recent work.[20] However, relatively little is understood about how the electrical conductivity of the nanostructured materials functions on flexible chemiresistor devices.[20−32] This understanding is important because the correlation between the electrical conductivity and the nanostructural parameters including particle size, interparticle distance, dielectric medium, and device strain is crucial for the design of sensing arrays on flexible devices. These parameters determine the activation energy in a thermally activated conduction path and thus have an important impact on the electrical signal amplification in sensing applications.

One of the important characteristics of the nanoparticle assembly on flexible electrical devices is the device strain effect on electrical conductivity as a result of bending or wrapping. There have been a few recent reports on this type of electrical−mechanical properties. In a recent study of mechanical flexibility of single-crystal transistors, the device field-effect mobility was found to change as a function of bending radius and strain.[39] When the substrate was bent from a radius of 7.4 to 5.9 mm, the mobility

* Address correspondence to cjzhong@binghamton.edu.

Received for review May 20, 2011 and accepted July 26, 2011.

**Published online August 02, 2011**
10.1021/nn201858c

dramatically drops more than 2 orders of magnitude. The bending was believed to induce a large interfacial strain on the crystal and possibly the dielectric, which results in a decrease of mobility.[39] In another study of the bending effect on the electrical properties of flexible organic thin film transistors on stainless steel substrates, the compressive strain was found to result in an increased mobility, while the tensile strain degraded the electrical performance.[31] The mechanical strains were believed to influence the energy barrier height between the grains of pentacene thin films, thereby resulting in the variation of channel resistances.[40] In another study, the graphene structure on a polyethylene terephthalate (PET) flexible substrate was demonstrated to function as a flexible and transparent electrode for field emission displays.[41] Thin films consisting of cross-linked nanoparticle aggregates have been shown to function as highly sensitive strain gauges which exploit the exponential dependence of the interparticle tunnel resistance on the particle separation.[42] Importantly, the modeling of the strain gauge behavior predicts the dependence of the gauge factor on several parameters, including the nanoparticle size, the interparticle separation gap, and the conductance of the linker molecules.[42]

These previous studies have demonstrated the importance of strain effect on flexible device performance. However, little has been addressed for one of the critical factors responsible for the strain-induced responses, such as the molecular atmosphere in the device strain environment. In a recent report of our preliminary work,[20] it was hypothesized that the resistance of nanoparticle thin film assemblies on flexible chemiresistor devices under strain could change significantly as a result of the change in dielectric properties. An in-depth investigation is thus needed for assessing the bending responses of the nanostructured flexible devices in different bending environment. In this report, we describe new findings of an investigation of the electrical conductivity properties of molecularly mediated thin film assemblies of nanoparticles on flexible chemiresistor devices under different conformal wrapping or bending conditions and different exposure molecules. One important focus is the understanding of the resistance dependence on the bending directions for the devices exposed to various gas/vapor molecules. The goal is to gain fundamental insights into the correlation between the electrical response characteristics of the detailed nanostructures and the device stain parameters.

## RESULTS AND DISCUSSION

**Theoretical Considerations.** Device bending was performed manually by wrapping the flexible device around a cylinder with a defined diameter. Figure 1A shows an example of the flexible sensor device coated

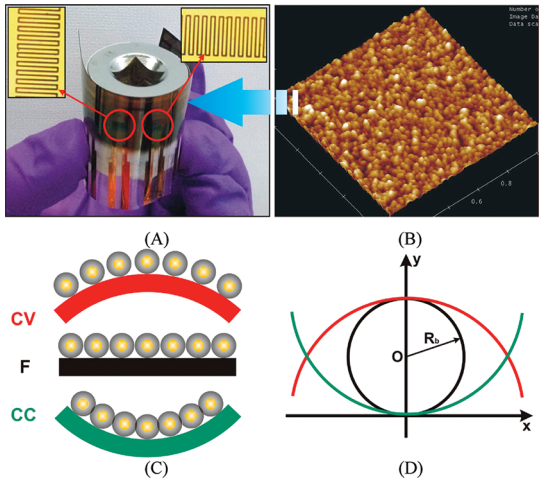


**Figure 1. (A) Photo of a flexible sensor device showing bending and the orientations of the interdigitated microelectrode patterns in the device relative to the device bending direction: "vertical" (upper-left corner) and "horizontal" (upper-right corner). (B) AFM image of NDT-$Au_{2nm}$ thin film. (C) Illustration of the two types of bending (F, flat; CC, concave (compressive strain); CV, convex (tensile strain)), and (D) definition of the radius of curvature ($R_b$) for the wrapping.**

with an NDT (1,9-nonadithiol)-linked Au nanoparticle (2 nm) thin film under concave wrapping, that is, tensile strain. Details for the quantitative analysis of the mechanisms for the molecularly mediated thin film assembly in terms of film mass or thickness growth kinetics were described in our previous reports.[5−7,17] As shown by the AFM image (Figure 1B), the thin film of nanoparticles displays a relatively uniform morphology. The NDT-linked DT-$Au_{2nm}$ (NDT-$Au_{2nm}$) thin films were assembled as sensing materials with a thickness of about 320 nm. The molecularly mediated thin film assemblies of gold nanoparticles by different linker molecules have been characterized in terms of thin film morphology, crystalline structure, nanoparticle ordering, interparticle molecular interaction, and interparticle distance properties using transmission electron microscopy, X-ray powder diffraction and grazing angle X-ray diffraction, FTIR, *etc.*, details of which were described in our previous reports.[5−7,11,17,19]

Two specific orientations of the interdigitated copper microelectrode lines in the flexible device were examined with respect to the wrapping direction: vertical and horizontal (Figure 1A). The thin film assembly on the microelectrode patterns undergoes compressive strain or tensile strain depending on the wrapping direction. The changes of the resistance in response to bending of the device were measured under different radius of curvature upon bending of the flexible device along the indicated directions, as shown in Figure 1C. For bending at specific radius of curvature ($R_b$) (Figure 1D), one cycle is defined as "flat−concave bending−flat−convex bending−flat" (F−C−F−V). The differential resistance changes ($\Delta R/R$) were measured in each cycle in terms of concave bending

("CC", *i.e.*, compressive strain) and convex bending ("CV", *i.e.*, tensile strain). The viability of the flexible device's tolerance toward bending or wrapping was also examined in multiple cycles of bending.

The overall electrical conduction (electron hopping and/or electron tunneling) of the nanostructured thin film assemblies on the flexible substrates depends on several nanostructural parameters such as particle core radius ($r$), interparticle distance ($d$), and dielectric constant of interparticle medium ($\varepsilon$). By controlling the number of methylene groups of the linking molecules and the particle sizes, the electrical conductivity of the nanoparticle thin film assemblies in the absence of device strains has been found to follow the thermally activated conduction pathway in which the activation energy increases with the interparticle distance and decreases with the particle size, details of which are described in our previous reports.[11,19] In the present study, the electrical conductivity *versus* device strain correlation for the flexible device coated with the nanoparticle thin film assemblies is the focus of our investigation. The relative change in electrical resistance or conductivity of the nanostructured thin films in response to conformal device bending is first modeled in terms of concave or convex wrapping of the device. The electrical conductivity of the thin films can be described by a thermally activated conduction path:[11,18,19]

$$\sigma = \sigma_0 \exp(-\beta d)\exp\left[-\frac{0.5e^2}{4\pi\varepsilon\varepsilon_0 RT}\left(\frac{1}{r}-\frac{1}{r+d}\right)\right] \quad (1)$$

where $e = 1.6 \times 10^{-19}$ C, $\varepsilon_0 = 8.854 \times 10^{-12}$ F/m, $R = 1.38 \times 10^{-23}$ J/K, $T = 300$ K, $\beta$ is the electron coupling term, and $r$ and $d$ represent particle radius and interparticle spacing (nm), respectively. In our previous study,[19] the electron coupling term ($\beta$) was shown to be dependent on particle size and relatively independent of the distance of the interparticle linkages. Assuming that the change of the interparticle distances from flat ($d_1$) to bent ($d_2$) is $\Delta L$ ($=d_2 - d_1$), the ratio of the electrical conductivity can be written as

$$\frac{\sigma_2}{\sigma_1} = \exp[-\beta(d_2-d_1)]\exp\left[\frac{0.5e^2}{4\pi\varepsilon\varepsilon_0 RT}\left(\frac{1}{r+d_2}-\frac{1}{r+d_1}\right)\right]$$

or

$$\frac{R_2}{R_1} = \frac{\sigma_1}{\sigma_2} = \exp[-\beta(d_1-d_2)]\exp\left[\frac{0.5e^2}{4\pi\varepsilon\varepsilon_0 RT}\left(\frac{1}{r+d_1}-\frac{1}{r+d_2}\right)\right] \quad (2)$$

This ratio contains two exponential components. The first component is mainly determined by the interparticle distance change and the $\beta$ value ($\beta-d$ component), whereas the second component is largely dependent on the particle size, interparticle distance change, and $\varepsilon$ value ($\varepsilon-r$ component). Assume that $\varepsilon = 10$ and $T = 300$ K, the $R_2/R_1$ ratio is derived as

$$\frac{R_2}{R_1} = \exp[\beta(d_2-d_1)]\exp\left[2.78\text{ nm}\times\left(\frac{1}{r+d_1}-\frac{1}{r+d_2}\right)\right] \quad (3)$$

Consider now the relative contributions of the above two components to the electrical conductivity of the thin films under different device strain effects. The $\beta-d$ component is largely determined by the strain effect ($\varepsilon_{strain}$)

$$\varepsilon_{strain} = \frac{\Delta L}{L} = \frac{d_2-d_1}{2r+d_1} = \frac{T_s}{2R_b} \quad (4)$$

where $L$ is the gap between the microelectrodes. For our nanoparticle thin film coated flexible PET substrate, the substrate thickness $T_s = 125\ \mu$m, the radius of bending $R_b = 5$ mm $= 5000\ \mu$m, $r = 1$ nm, and $d_1 = 1.6$ nm. In our earlier report,[19] we obtained $\beta = 4.0$ nm$^{-1}$. Substituting these values into the equation, we can express the $\Delta R/R_1$ ratio as a function of strain, $\varepsilon_{strain}$

$$\frac{\Delta R}{R_1} = \frac{R_2-R_1}{R_1} = \exp[3.6\times\beta\varepsilon_{strain}]\exp\left[2.78\times\left(\frac{1}{2.6}-\frac{1}{2.6+3.6\times\varepsilon_{strain}}\right)\right]-1 \quad (5)$$

In this case, $\Delta R/R_1$ would be dependent on $\varepsilon_{strain}$. Figure 2A shows the plot of $\Delta R/R_1$ *versus* $\varepsilon_{strain}$ for both convex (tensile strain) and concave (compressive strain) wrapping directions. There are three observations. First, $\Delta R/R_1$ increases with $\varepsilon_{strain}$. Second, the magnitude of $\Delta R/R_1$ is larger for tensile strain than that for compressive strain. Third, the magnitude of $\Delta R/R_1$ depends on particle size and $\beta$ value. $\Delta R/R_1$ is greater for larger sized particles if all other parameters are fixed. At fixed particle size, $\Delta R/R_1$ is greater for a larger $\beta$ value.

For the $\varepsilon-r$ component, we consider the possible change of $\varepsilon$ due to the filling in the interparticle void spaces with gas/vapor molecules as a result of device exposure in different bending environment. The derived changes in electrical resistance for CV and CC wrapping directions are

$$\frac{\Delta R}{R_{1\,(CV)}} = \exp[900/R_b]\exp\left[\frac{27.8\text{ nm}}{\varepsilon}\times\left(\frac{1}{2.6}-\frac{1}{2.6+\frac{225}{R_b}}\right)\right]-1 \quad (6a)$$

$$\frac{\Delta R}{R_{1\,(CC)}} = \exp[-900/R_b]\exp\left[\frac{27.8\text{ nm}}{\varepsilon}\times\left(\frac{1}{2.6}-\frac{1}{2.6-\frac{225}{R_b}}\right)\right]-1 \quad (6b)$$

In this case, $\Delta R/R_1$ would be dependent on $\varepsilon$ under a fixed $R_b$. Figure 2B shows the plots of $\Delta R/R_1$ *versus* $R_b$ for both convex (tensile strain) and concave (compressive

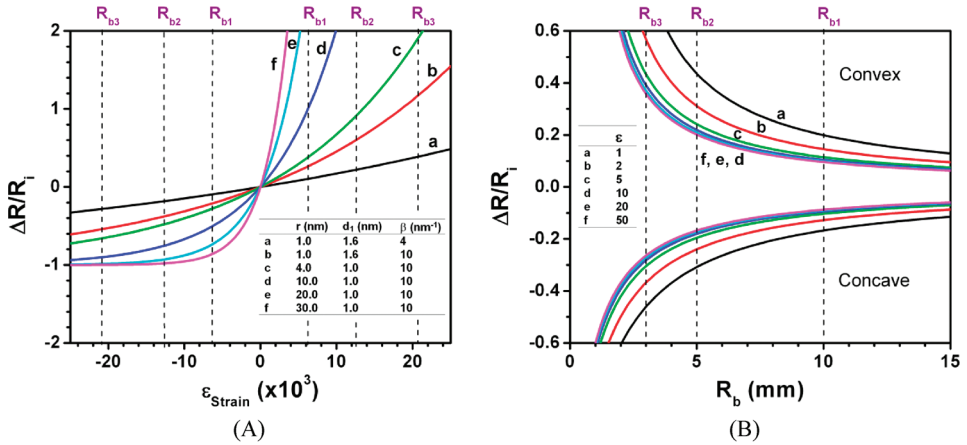


**Figure 2. Plots of $\Delta R/R_1$ *vs* $\varepsilon_{strain}$ based on eq 5 (A; $\varepsilon = 10$), and $\Delta R/R_1$ *vs* radius of curvature for the bending ($R_b$) based on eq 6 (B; $r = 1.0$ nm, $d_1 = 1.6$ nm, $\beta = 4.0$ nm$^{-1}$) for both convex (tensile strain) and concave (compressive strain) wrapping directions. The dashed lines represent data for $R_{b1} = 10$ mm, $R_{b2} = 5$ mm, and $R_{b3} = 3$ mm.**

strain) wrapping directions. In addition to the observation of $\Delta R/R_1$ increase with $R_b$, and the opposite signs for both convex (tensile strain) and concave (compressive strain) wrapping directions, the magnitude of $\Delta R/R_1$ decreases with the increase of $\varepsilon$.

**Response Characteristics to Different Vapors under No Device Strain.** The electrical conductivity of the flexible device under no device strain in response to exposures to vapors with different dielectric constants was first examined. Figure 3 shows a representative set of the sensor response ($\Delta R/R$ where $R$ represents $R_1$) and sensitivity profiles for NDT-$Au_{2nm}$ (Figure 3A) and MUA (11-mercaptoundecanoic acid)-linked Au nanoparticle (MUA-$Au_{2nm}$) (Figure 3B) films in response to hexane and water vapors. Glass substrate was used in this case to ensure absolutely no device strain. The response profile features an increase in absolute value of $\Delta R/R$ upon exposure to vapor which returns to baseline upon purge with nitrogen. The response is rapid and reversible. In most cases, the responses increased linearly with vapor concentration when the concentration was not too high. The slope serves as a measure of the response sensitivity. Deviation from the linear relationship occurs when the vapor concentration is above a certain value, the exact value of which depends on the vapor. Such a deviation is due to the existence of a saturation effect and or the complication of both bulk and surface adsorption phenomena.[10,11] For the convenience of an overall assessment of the data, we used the linear approximation for assessing the response data. In general, the response sensitivities of MUA-$Au_{2nm}$ are higher than those of NDT-$Au_{2nm}$ films to vapors on the same channel because of the correlation of the electrical signals depending on the three nanostructural parameters, $r$, $d$, and $\varepsilon$. An important finding from Figure 3A,B is that the devices exhibited an opposite response characteristic between the two different films for water vapor. In contrast to the small positive response characteristic observed for the NDT-$Au_{2nm}$ film, the data for the MUA-$Au_{2nm}$ film showed a negative trend in response.

The understanding of how dielectric constants of the analytes correlate with sensor responses is important because the electrical conductivity is dependent on the dielectric properties of the thin film in a significant way. The basic concept is that the dielectric constant of the nanostructured sensing thin film may change as a result of the sorption of the vapor with different dielectric constants. Since the sorption of vapors in the nanostructured film is expected to increase the dielectric constant of the thin film materials, the response of the thin films to vapors with low dielectric constant could be very different from those for vapors with high dielectric constants. We examined the response characteristics of the nanostructured sensing thin films in response to a number of volatile organic compounds with different dielectric constants, including hexane, ethanol, methanol, acetonitrile, water, *etc.* In contrast to vapors such as hexane, which has a very low dielectric constant ($\varepsilon \sim 2$), vapors such as ethanol, methanol, acetonitrile, and water exhibit $\varepsilon$ values ranging from 20 to 80. The response profiles of the MUA-$Au_{2nm}$ thin film revealed a remarkable positive−negative switching characteristic between positive and negative response profiles. When the signs and the magnitudes of the response sensitivities of each device in response to the vapors with different dielectric constants were compared (Figure 3C), one of the most important observations was the dependence of the response sensitivities on the dielectric constants of the vapor.

In general, the change in resistance decreases with the increase in $\varepsilon$ of the vapors, which is qualitatively consistent with the theoretical trend. When $\varepsilon$ is increased to above 30−40, the switching from the usual positive response to the negative response characteristic becomes evident. In addition, the magnitude of the response also seems to show such a remarkable

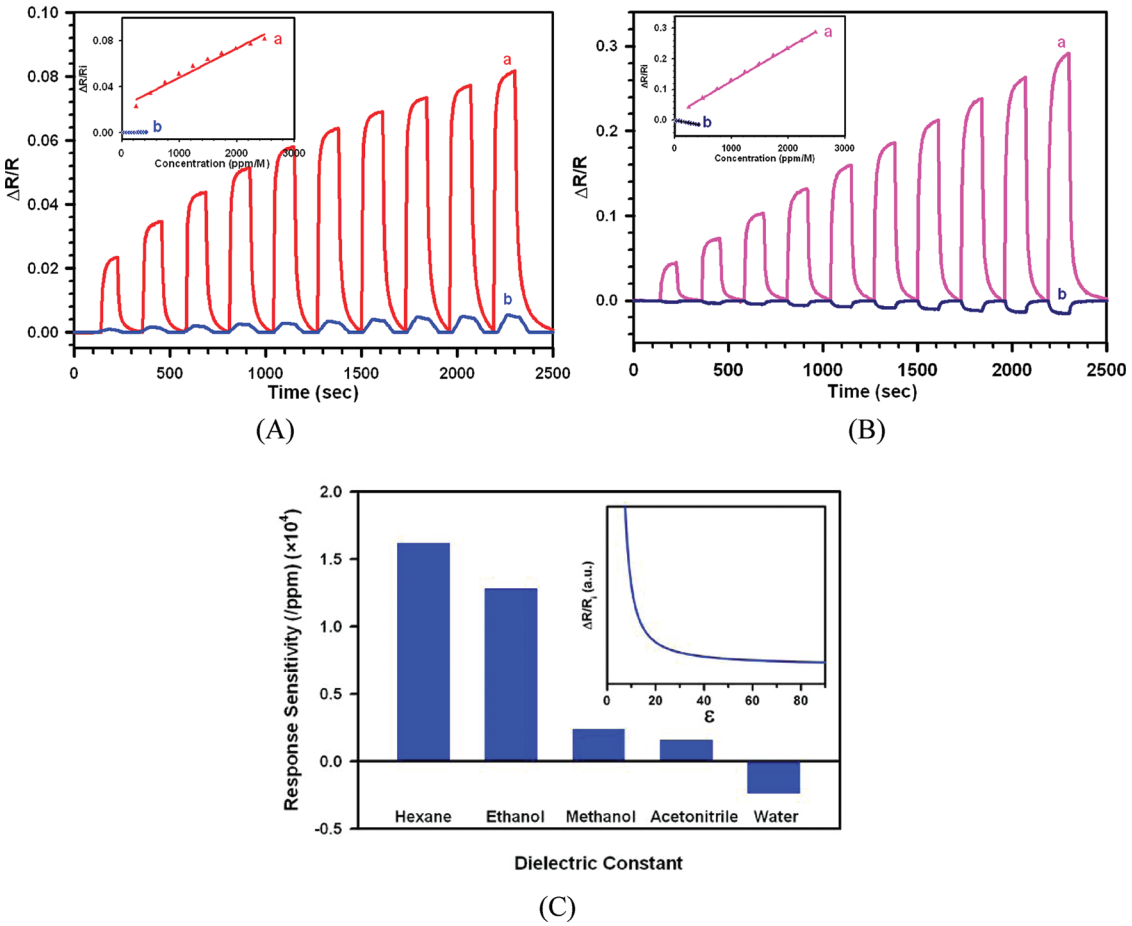


**Figure 3. (A,B) Response profiles and response sensitivities for chemiresistor devices with NDT-$Au_{2nm}$ film (A) and MUA-$Au_{2nm}$ film (B) in response to hexane (a) and water (b) vapors (the response of NDT-$Au_{2nm}$ to water was multiplied by a factor of 10 in A). Inset in A: Sensitivity for NDT-$Au_{2nm}$ film = $2.5 \times 10^{-5}$ ($ppm^{-1}$) (a) and $1.2 \times 10^{-6}$ ($ppm^{-1}$) (b). Inset in B: Sensitivity for MUA-$Au_{2nm}$ film = $1.1 \times 10^{-4}$ ($ppm^{-1}$) (a) and $-3.5 \times 10^{-5}$ ($ppm^{-1}$) (b). (C) Comparison of response sensitivities upon exposure to different vapors: hexane ($\varepsilon$ = 1.9), ethanol ($\varepsilon$ = 25.3), methanol ($\varepsilon$ = 33.0), acetonitrile ($\varepsilon$ = 36.6), and water ($\varepsilon$ = 80.1). Inset in C: Theoretical prediction of $\Delta R/R$ *vs* $\varepsilon$ based on eq 1. The vapor concentration is given in the unit of ppm moles per liter (ppm (M)), which can be converted to ppm (V) by multiplying a factor of 24.5.[11]**

trend: it increases with the decrease of the dielectric constant for vapors with the lower dielectric constants; it increases with $\varepsilon$ for vapors with higher dielectric constants. This finding shows that the change of the vapor adsorption induced changes in dielectric properties in the nanostructured thin film plays a key role in the nanoparticle-structured sensor response characteristics.

**Response Characteristics under Device Wrapping/Bending Strains.** The response characteristics upon device bending were examined under different radii of curvatures and different vapor exposure environments, including nitrogen, hexane, ethanol, acetonitrile, and water vapors. The selection of these vapors was based on the differences in a combination of the molecular polarity, hydrophobicity/hydrophilicity, and dielectric constant. The results are discussed below in terms of response characteristics under small device strain, large device strain, and different device bending orientations with respect to the microelectrode orientation.

First, the device response characteristics are compared between the resistance response data obtained under nitrogen (dry environment) and those obtained upon device exposure to different vapor molecules under relatively small device strain, that is, $R_b \geq 10$ mm (or strain $\varepsilon_{strain} \leq 6.3 \times 10^{-3}$). Figure 4A shows a representative set of $\Delta R/R$ *versus* bending ($R_b$ = 10 mm) under nitrogen atmosphere for a device coated with NDT-$Au_{2nm}$ film. The value of $\Delta R/R$ is negative for the concave bending and positive for the convex bending. The average value of $\Delta R/R$ was found to be $-0.57$ for the concave bending and 0.52 for the convex bending. While there are small variations, a consistent response pattern is evident in which the concave bending decreases the resistance, whereas the convex bending increases the resistance.

Figure 4B shows the $\Delta R/R$ change of the same device under water vapor (RH = 86%). In sharp contrast to the results under the relatively dry condition, the resistance was found to decrease for both the concave and convex bending under the relatively humid testing

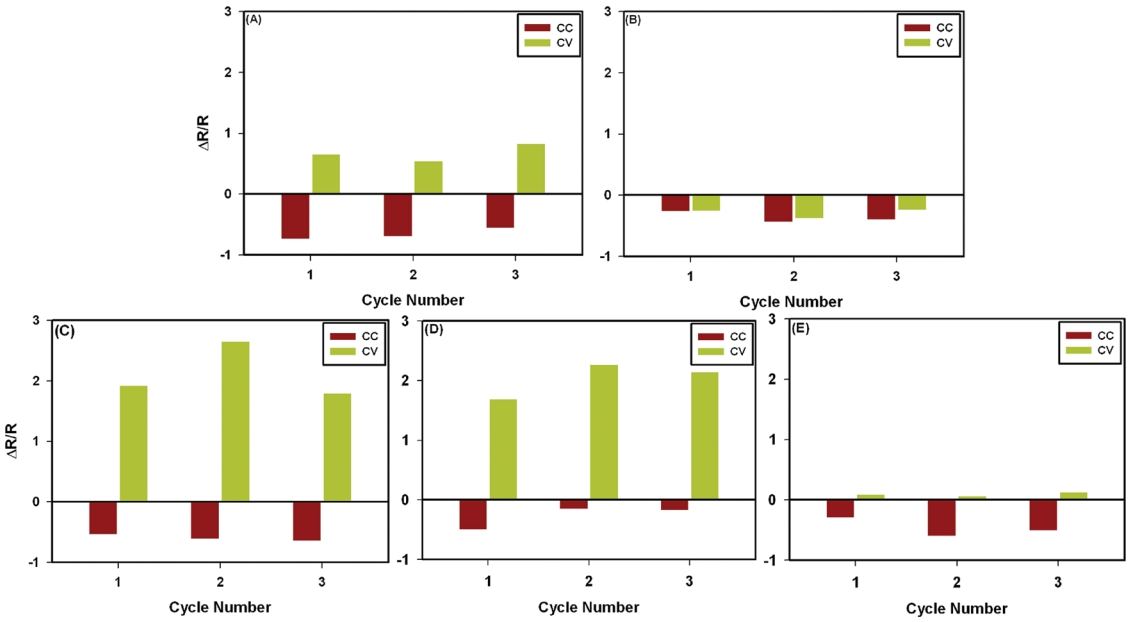


**Figure 4. Differential resistance change, $\Delta R/R$, of a device coated with NDT-$Au_{2nm}$ film in response to repetitive flat *vs* bending cycles for a device ($R_b$ = 10 mm) with the microelectrode pattern in the "vertical" orientation under nitrogen (dry) (A), water (RH = 86%) (B), hexane (~4100 ppm, C), ethanol (~1600 ppm, D), and acetonitrile (~2800 ppm, E).**

environment. The average value of $\Delta R/R$ was −0.37 for the concave bending and −0.30 for the convex bending. The trends of the resistance change for the bending are the same for all of the measurements repeated in several days.

The response patterns were further examined under other vapors, including hexane, ethanol, and acetonitrile, with dielectric constants falling between nitrogen and water vapors (Figure 4C−E). For repetitive bending cycles of the device under hexane, the resistance was found to decrease for the concave bending and increase for the convex bending (Figure 4C). The value of $\Delta R/R$ was found to be negative for the concave bending, suggesting the decreasing resistance, and positive for the convex bending, suggesting the increasing resistance. The average value of $\Delta R/R$ was −0.55 for concave bending and 2.1 for convex bending.

For device bending under ethanol, similarly, the resistance was found to decrease for concave bending and increase for convex bending (Figure 4D). The average value of $\Delta R/R$ was −0.16 for concave bending and 2.0 for convex bending. For device bending under acetonitrile (Figure 4E), the value of $\Delta R/R$ was found to be negative for the concave bending and positive for the convex bending, the latter of which is much smaller than those under hexane and ethanol, exhibiting an average $\Delta R/R$ value of −0.46 for concave bending and 0.071 for convex bending.

In Figure 5, the average values of $\Delta R/R$ obtained for different bending directions under different gas/vapor molecules are compared. In general, the concave bending decreases the resistance, whereas the convex bending increases. However, the magnitudes are different depending on the gas/vapor environment. The data showed the highest change for hexane and ethanol vapors. There appears to be a trend of decrease with increasing dielectric constant of the vapors for convex bending, exhibiting a negative $\Delta R/R$ response for water vapor. For concave bending, the $\Delta R/R$ responses appear to show little dependence on the vapor environment.

As shown in the theoretical modeling, $\Delta R/R$ depends on a combination of $\varepsilon$ and $R_b$. Under all conditions except for water vapor, the concave wrapping decreases the resistance whereas convex bending increases the resistance, which is clearly consistent with the theoretical modeling. Under the humid condition, both concave bending and convex bending decrease the resistance. The trend of $\Delta R/R$ decrease with increasing dielectric constant of the vapors for convex bending, including the negative $\Delta R/R$ response for water vapor, does not seem to be explainable by the strain-dependent theoretical consideration (eq 5). Rather, the $\varepsilon$-dependent theoretical consideration (eq 6) seems to provide a good explanation of the trend. For hexane and ethanol vapors, the magnitude of the $\Delta R/R$ responses seems to be much larger (by a factor of ~10) than the theoretical changes using either strain- or $\varepsilon$-dependent theoretical responses ($\Delta R/R$ = 0.1−0.2). In contrast to convex bending in which more air can be accommodated in the enlarged interparticle voids leading to an increased resistance, there is less air ($\varepsilon \approx 1$) between the particles for the case of concave bending. The average dielectric median constant is expected to increase. Therefore, concave bending leads to an increased conductivity.

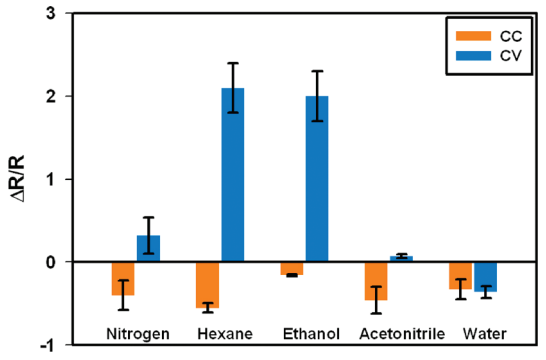


**Figure 5. Comparison of average $\Delta R/R$ values in response to convex and concave bending of a device coated with NDT-$Au_{2nm}$ film ($R_b$ = 10 mm) under different gas/vapor molecules.**

Under water vapor, the concave bending leads to the expulsion of air between the interparticle voids because the interparticle spacing decreases. The concave bending under the high relative humidity increases the conductivity, similar to the result under dry conditions. The convex bending enlarges the interparticle voids, leading to an increase of water molecules flowing into the interparticle voids. The dielectric constant of water vapor is much larger than air and the organic medium in the film, resulting in an increase of the average dielectric medium constant. This large increase is clearly associated with the observation of the negative $\Delta R/R$ values for water vapor. The tests with the other vapors substantiate the assessment. Hexane and ethanol have great solubility in the NDT-Au film, which qualitatively explains the large resistance increase. Acetonitrile is a polar molecule and does not have high solubility in the film, which qualitatively explains the small resistance increase. In comparison with the data under no device strain, where similar dependence on dielectric constant was observed (see Figure 3C), the finding suggests that the bending responses of electric conductivity under the relatively large radius of curvature is likely dominated by dielectric constant, while the device strain plays an additional role in fine-tuning the electrical properties.

Second, the bending response was further examined under relatively large device strains or smaller radii of curvature, such as $R_b$ < 10 mm (or strain $\varepsilon_{strain} > 6.3 \times 10^{-3}$). For example, under different gases/vapors for $R_b$ = 3 mm, the resistance was found to decrease upon concave bending whereas it increased upon convex bending (see Figure S1 in the Supporting Information), consistent with the data obtained under $R_b$ = 10 mm, except for the water vapor. While there were variations from measurement to measurement due to the lack of precise control of the radius of curvature, the above response characteristics were clearly reproducible. Under dry condition, the average value of $\Delta R/R$ was found to be −0.19 for the concave bending and 0.23 for the convex bending. For hexane vapor, the average value of $\Delta R/R$ was −0.77 for the concave bending and 0.49 for the convex bending. For ethanol vapor, the average value of $\Delta R/R$ was −0.53 for the concave bending and 0.51 for the convex bending. For acetonitrile vapor, the average value of $\Delta R/R$ was −0.54 for the concave bending and 0.43 for the convex bending. For water vapor, the resistance was found to decrease for the concave bending and increase for the convex bending, in contrast to the resistance to the decrease for the convex bending under $R_b$ = 10 mm. The average value of $\Delta R/R$ was −0.30 for concave bending and 0.20 for convex bending, which is quite close to those found under nitrogen conditions.

The above data of resistance changes are compared in Figure 6. In comparison with those obtained at $R_b$ =10 mm, both concave and convex bending data at $R_b$ = 3 mm are again qualitatively consistent with the results of the theoretical modeling.

The trend of the $\Delta R/R$ decrease with increasing dielectric constant of the vapors for both convex and concave bending seems to be explainable by the $\varepsilon$-dependent theoretical consideration (eq 6). However, the magnitude of the $\Delta R/R$ changes seems to be smaller than the $\varepsilon$-dependent theoretical prediction. The magnitude of the $\Delta R/R$ changes is smaller than those under $R_b$ = 10 mm, which seems quite close to the strain-dependent theoretical consideration (eq 5). This finding suggests that the bending responses under small radius of curvature is likely dominated by device strain, while the dielectric constant plays an additional role in fine-tuning the electrical properties.

Lastly, we further compared responses of devices with two different microelectrode orientations, that is, "vertical" and "horizontal", as illustrated in Figure 1A for bending under relatively small radius of curvature ($R_b$ = 5 mm) for ethanol and acetonitrile vapors that have both polarity and dielectric constant falling between hexane and water. The responses are compared between horizontal (device A) and vertical (device B), along with the responses under nitrogen (see Figure S2 in the Supporting Information). Under nitrogen (a), device A exhibits an average $\Delta R/R$ of −0.19 for the concave bending and 0.09 for the convex bending, whereas device B shows average $\Delta R/R$ of −0.23 for the concave bending and 0.06 for the convex bending. The differences between these two microelectrode pattern orientations are apparently very small under nitrogen.

In comparison with the responses under nitrogen, significant differences have been observed between these two microelectrode pattern orientations under ethanol and acetonitrile. For ethanol (c), device A exhibits an average $\Delta R/R$ of −0.07 for the concave bending and 0.056 for the convex bending, whereas device B shows an average $\Delta R/R$ of −0.29 for the concave bending and 1.2 for the convex bending. For acetonitrile (a), device A exhibits an average $\Delta R/R$ of −0.08 for the concave bending and 0.088 for the convex bending, whereas device B shows average

$\Delta R/R$ of −0.56 for the concave bending and 0.28 for the convex bending. Note that device B tested under $R_b$ = 5 mm has the same microelectrode orientation as the devices tested under $R_b$ = 10 and 3 mm. The responses of device B are largely consistent with the expected trend, with some variations due to subtle differences of the microelectrode parameters from device to device.

The above resistance changes are compared in Figure 7. The differences between these two microelectrode pattern orientations are apparently very small under nitrogen, which appear to be consistent with the theoretical predictions for both strain-induced and dielectric constant-induced changes in resistance. However, there appear to be significant differences between the same two devices under ethanol and acetonitrile. The magnitude of the responses is smaller for the horizontal orientation than those for the vertical orientation (by a factor of 3−20 depending on the vapor molecule nature and the bending direction).

Theoretically, if the nanoparticle assembly has no specific ordering with respect to the microelectrode orientation, which appears to be the likely morphology, one would not expect any difference between the two orientations because of their identical strain. This is indeed true for the results obtained under nitrogen.

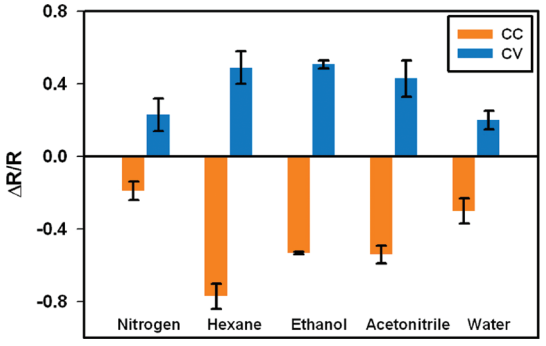


**Figure 6. Comparison of average $\Delta R/R$ values in response to convex and concave bending of a device coated with NDT-$Au_{2nm}$ film ($R_b$ = 3 mm) under different gas/vapor molecules.**

However, under ethanol and acetonitrile, the observation of the difference suggests other possible factors. One possibility is that there is some degree of ordering for the nanoparticles in the thin film, and thus the strain-induced change of interparticle distances would be different between the two microelectrode orientations. Scheme 1 depicts an idealized model for the nanoparticles in the thin film assembly (*e.g.*, (100) packing of the assembled nanoparticles). This model illustrates how the interparticle distances for the device with vertical microelectrode orientation under the same device bending direction would be different from that for the device with a horizontal orientation. In this case, the interparticle distance for the device with horizontal microelectrode orientation would increase more than that for the device with vertical microelectrode orientation under the same strain, which would increase the conductivity more significantly for the former case. This is, however, the opposite of the experimental observation under the two vapors for the bending of the two different microelectrode orientations.

Another possibility is that the change of the dielectric properties in the film could operate in such a way that the ordered interparticle spatial characteristic, as shown in Scheme 1c, would favor the enhancement in dielectric effect of the solvent molecules on the surface conductivity in comparison to that shown in Scheme 1b. We do not have direct evidence at this point, but one hypothesis is that the more effective increase of dielectric constant in the film in Scheme 1c leads to resemblance of the surface to a layer of the adsorbed molecules. This type of resemblance would lead to a higher surface conductivity resembling ionic conductor, not electronic conductor, which could play a role in producing a more effective increase of the resistance in the case of Scheme 1c because of a better continuity of the molecules between the two microelectrodes. In this case, the higher the dielectric constant, the less conductance the film has. Within the two-microelectrode confinement, the film with a higher dielectric constant

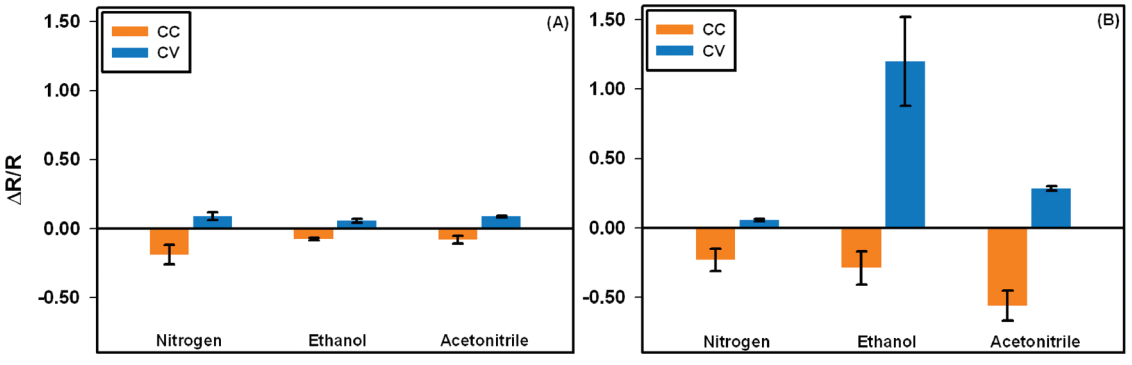


**Figure 7. Comparison of the average $\Delta R/R$ values in response to convex and concave bending for two devices coated with NDT-$Au_{2nm}$ films ($R_b$ = 5 mm) but with the microelectrode patterns in two different orientations with respect to the bending direction, horizontal (A) and vertical (B), under different gas/vapor molecules.**

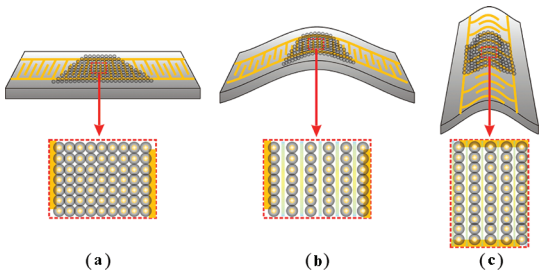


**Scheme 1. Illustrations of possible changes in interparticle distances for a microelectrode pattern on a flexible device without strain (a) and with strain (b and c). Under device strain, the interparticle spatial properties may change differently for the two orientations of the microelectrode pattern with respect to device bending directions: horizontal (b) and vertical (c).**

will conduct less because of a greater buildup of opposite charges on the two microelectrodes, which in fact results in a greater capacitance. This could be qualitatively explained by considering the capacitive characteristic of the surface with a layer of polar solvents, $C = Q/V$, where $C = \varepsilon (A/L)$ ($\varepsilon$, dielectric constant of the fluid molecules; $A$, area of the electrodes; $Q$, change on the electrodes; and $V$, voltage across the electrodes). The voltage buildup would be $V = (Q/\varepsilon)(L/A)$, which is opposite of the applied voltage for the resistance measurement. This more effective voltage buildup leads to an enhanced resistance of the film for the case of the vertical orientation than the horizontal orientation under the convex bending. Under concave bending, the reduced interparticle void space should then diminish the difference observed under the convex bending. This trend seems to be observed in the data for ethanol but not in the data for acetonitrile. To fully explain these differences, an in-depth impedance study of the electrical and capacitive properties of the thin films under the different bending and different vapors will be needed. In this study, the nanoparticle thin film assembly between the two microelectrodes is modeled by an equivalent circuit represented by a parallel combination of resistances and capacitances. The resistive and capacitive components can be distinguished by analysis of complex plane impedance spectra, which is part of our ongoing work.

## CONCLUSIONS

In conclusion, the electrical characteristics of the nanoparticle thin film assembly on flexible chemiresistor devices have been found to depend on a combination of the device strain and the exposure molecular environment. This dependence has been established by both theoretical modeling and experimental data. Under no device strain, the electrical conductivity is highly sensitive to the molecular nature in the exposure gas/vapor environment, revealing a clear increase in electrical conductivity with dielectric constant of the vapor molecules. Under small device strains, the electrical conductivity is shown to respond sensitively to the strain directions (tensile *vs* compressive strain) and also to the dielectric constant of the vapor molecules in a way similar to the characteristic observed under no device strain. Under relatively large device strains, the electrical conductivity is shown to respond to the change in dielectric constant of the vapor molecules but more significantly to the device tensile and compressive strains than those under small device strains. This combination of device strain and dielectric characteristic is further shown to be dependent on the orientation of the microelectrode patterns with respect to the device strain direction. These findings have demonstrated how wrapping or bending influences the interparticle packing, ordering, and spatial structures of nanoparticle assemblies on flexible devices in the presence of gas/vapor molecules. These findings, upon gaining a further mechanistic insight into the structural and morphological changes of the thin films, will have important implications for the design of nanostructured flexible devices for sensing applications which require conformal wrapping or bending adaptability in various complex or special sensing environments.

## EXPERIMENTAL METHODS

**Chemicals and Nanoparticles.** Hydrogen tetrachloroaurate trihydrate (99%), tetraoctylammonium bromide (99%), decanethiol (DT, 96%), sodium borohydride (99%), 1,9-nonadithiol (NDT, 95%), and 11-mercaptoundecanoic acid (MUA, 95%) were obtained from Aldrich. Solvents included hexane (99.9%), toluene (99.9%), methanol (99.9%), acetonitrile (99.8%), and ethanol (99.9%) from Aldrich. Water was purified with a Millipore Milli-Q water system.

Gold nanoparticles of 2 nm diameter ($Au_{2nm}$) encapsulated with decanethiolate monolayer shells were synthesized by two-phase reduction of $HAuCl_4$ according to Brust's two-phase protocol[43] and a synthetic modification.[44] The as-synthesized gold nanoparticles (DT-$Au_{2nm}$) had an average size of 2.0 $\pm$ 0.7 nm. Gold nanoparticles with larger sizes were synthesized by a thermally activated processing route developed in our laboratory. Briefly, the solution containing the as-synthesized DT-$Au_{2nm}$ nanoparticles from the synthesis was heated at 150 °C to produce larger sized Au nanoparticles. Gold nanoparticles of 7.0 $\pm$ 0.5 nm diameters ($Au_{7nm}$) produced by this method were used in this work. Details for the morphology and size distribution can be found in previous reports.

**Preparation of Molecularly Mediated Thin Film Assemblies of Nanoparticles.** The DT-capped Au nanoparticles were assembled on the flexible chemiresistor devices using molecularly mediated interparticle linking. For example, NDT-linked thin films (NDT-$Au_{2nm}$) were prepared *via* an exchanging−cross-linking−precipitation route using a $10^3$−$10^4$ ratio of NDT to Au nanoparticles.[6,7] Briefly, a flexible device was immersed into the solution of NDT-$Au_{2nm}$ nanoparticles and NDT at room temperature for a controlled period of time, during which the solvent evaporation was prevented in the film formation. The resulting film-coated

device was rinsed many times to remove any unassembled components and dried using nitrogen gas.

**Device Fabrication.** Interdigitated copper microelectrodes were patterned on polyethylene terephthalate (PET) (DuPont Tejin Films Melinex ST507) film with 125 $\mu$m thickness. The PET sheets were cleaned using isopropyl alcohol and oxygen plasma before sputtering of 5 nm Cr and 300 nm Cu films. The Cu microelectrode parameters are 400 $\mu$m for finger length, and 10 $\mu$m for finger spacing, and 10 $\mu$m for finger width. The total number of microelectrodes is 300 for each of the devices. The microelectrode devices feature 150 pairs of microelectrodes with well-defined length, width, and spacing. Some details for the microfrabrication were reported previously.[11,19−20]

**Measurements.** A 2000 mL of glass container (test chamber) was cleaned by distilled water and dried by $N_2$ gas. A humidity meter (USB-502-LCD) was taped on the wall of a glass container. A $5' \times 4'$ parafilm was cut and stretched to cover the container. The test chamber was purged with $N_2$ through the parafilm to lower the humidity. The device was connected to the computer-interfaced multichannel meter (Keithley, Model 2700) to measure the resistance. The resistances were measured in the wrapping orders of flat, concave, flat, and convex. The wrapping was controlled manually using a cylinder with well-defined diameter. In the case of manual operation, we measured the radius of curvature using a ruler, which had a possible variation of about 15%. The measuring steps above were repeated several times. After the experiment under relatively dry testing conditions was done, 200 mL of distilled water was added to the beaker, and a stirring bar was put in the beaker. When the humidity reached the maximum for 20 min, the measurements in response to the wrapping were tested. The same steps were repeated for device A and device B.

A Multimode Nano-Scope IIIa (Digital Instruments, Santa Barbara), equipped with an E scanner (maximum scan size = 16 $\mu$m), was utilized for AFM imaging. The capability of tapping mode (TM) AFM allows for imaging with minimum disruption to the nanostructures. Standard silicon tapping cantilevers (nanosensors) were used with a force constant of 40 N/m (TESP). The probe has a nominal tip radius with a curvature of ~10 nm. All images were acquired in TM. The instrument was calibrated by imaging standard calibration gratings.

*Acknowledgment.* The work is supported by NSF (CHE 0848701 and CMMI 1100736) and the Center for Advanced Microelectronics Manufacturing at SUNY Binghamton. The authors acknowledge the help from Dr. H. Zhang in the flexible device fabrication.

*Supporting Information Available:* Additional data of the electrical resistance measurements. This material is available free of charge *via* the Internet at http://pubs.acs.org.

## REFERENCES AND NOTES

1. Wohltjen, H.; Snow, A. W. Colloidal Metal−Insulator−Metal Ensemble Chemiresistor Sensor. *Anal. Chem.* **1998**, *70*, 2856–2859.
2. Murray, R. W. Nanoelectrochemistry: Metal Nanoparticles, Nanoelectrodes, and Nanopores. *Chem. Rev.* **2008**, *108*, 2688–2720.
3. Severin, E. J.; Lewis, N. S. Relationships among Resonant Frequency Changes on a Coated Quartz Crystal Microbalance, Thickness Changes, and Resistance Responses of Polymer−Carbon Black Composite Chemiresistors. *Anal. Chem.* **2000**, *72*, 2008–2015.
4. Lim, S.; Zhong, C. J. Molecularly Mediated Processing and Assembly of Nanoparticles: Exploring the Interparticle Interactions and Structures. *Acc. Chem. Res.* **2009**, *42*, 798–808.
5. Wang, L. Y.; Luo, J.; Schadt, M. J.; Zhong, C. J. Thin Film Assemblies of Molecularly-Linked Metal Nanoparticles and Multifunctional Properties. *Langmuir* **2010**, *26*, 618–632.
6. Leibowitz, F. L.; Zheng, W. X.; Maye, M. M.; Zhong, C. J. Structures and Properties of Nanoparticle Thin Films Formed *via* a One-Step Exchange−Crosslinking−Precipitation Route. *Anal. Chem.* **1999**, *71*, 5076–5083.
7. Han, L.; Maye, M. M.; Leibowitz, F. L.; Ly, N. K.; Zhong, C. J. Quartz-Crystal Microbalance and Spectrophotometric Assessments of Inter-Core and Inter-Shell Reactivities in Nanoparticle Film Formation and Growth. *J. Mater. Chem.* **2001**, *11*, 1258–1264.
8. Zheng, W. X.; Maye, M. M.; Leibowitz, F. L.; Zhong, C. J. Imparting Biomimetic Ion-Gating Recognition Properties to Electrodes with Hydrogen-Bonding Structured Core−Shell Nanoparticle Network. *Anal. Chem.* **2000**, *72*, 2190–2199.
9. Han, L.; Luo, J.; Kariuki, N.; Maye, M. M.; Jones, V. W.; Zhong, C. J. Novel Interparticle Spatial Properties of Hydrogen-Bonding Mediated Nanoparticle Assembly. *Chem. Mater.* **2003**, *15*, 29–37.
10. Han, L.; Daniel, D. R.; Maye, M. M.; Zhong, C. J. Core−Shell Nanostructured Nanoparticle Films as Chemically Sensitive Interfaces. *Anal. Chem.* **2001**, *73*, 4441–4449.
11. Wang, L. Y.; Shi, X.; Kariuki, N. N.; Schadt, M.; Wang, G. R.; Rendeng, Q.; Choi, J.; Luo, J.; Lu, S.; Zhong, C. J. Array of Molecularly Mediated Thin Film Assemblies of Nanoparticles: Correlation of Vapor Sensing with Interparticle Spatial Properties. *J. Am. Chem. Soc.* **2007**, *129*, 2161–2170.
12. Ibanez, F. J.; Zamborini, F. P. Chemiresistive Sensing of Volatile Organic Compounds with Films of Surfactant-Stabilized Gold and Gold−Silver Alloy Nanoparticles. *ACS Nano* **2008**, *2*, 1543–1552.
13. Zamborini, F. P.; Smart, L. E.; Leopold, M. C.; Murray, R. W. Distance-Dependent Electron Hopping Conductivity and Nanoscale Lithography of Chemically-Linked Gold Monolayer Protected Cluster Films. *Anal. Chim. Acta* **2003**, *496*, 3–16.
14. Cai, Q. Y.; Zellers, E. T. Dual-Chemiresistor GC Detector Employing Monolayer-Protected Metal Nanocluster Interfaces. *Anal. Chem.* **2002**, *74*, 3533–3539.
15. Grate, J. W.; Nelson, D. A.; Skaggs, R. Sorptive Behavior of Monolayer-Protected Gold Nanoparticle Films: Implications for Chemical Vapor Sensing. *Anal. Chem.* **2003**, *75*, 1868–1879.
16. Joseph, Y.; Guse, B.; Vossmeyer, T.; Yasuda, A. Gold Nanoparticle/Organic Networks as Chemiresistor Coatings: The Effect of Film Morphology on Vapor Sensitivity. *J. Phys. Chem. C* **2008**, *112*, 12507–12514.
17. Wang, L. Y.; Miller, D.; Fan, Q.; Luo, J.; Schadt, M.; Rendeng, Q.; Wang, G. R.; Wang, J.; Kowach, G. R.; Zhong, C. J. Assessment of Morphological and Optical Properties of Molecularly Mediated Thin Film Assembly of Gold Nanoparticles. *J. Phys. Chem. C* **2008**, *112*, 2448–2455.
18. Abeles, B.; Cheng, P.; Coutts, M. D.; Arie, Y. Structure and Electrical Properties of Granular Metal Films. *Adv. Phys.* **1975**, *24*, 407–46.
19. Wang, G. R.; Wang, L. Y.; Rendeng, Q.; Wang, J.; Luo, J.; Zhong, C. J. Correlation between Nanostructural Parameters and Conductivity Properties for Molecularly Mediated Thin Film Assemblies of Gold Nanoparticles. *J. Mater. Chem.* **2007**, *17*, 457–462.
20. Wang, L.; Luo, J.; Yin, J.; Wu, J.; Shi, X.; Crew, E.; Xu, Z.; Qiang, R.; Lu, S.; Poliks, M.; *et al.* Flexible Chemiresistor Sensors: Thin Film Assemblies of Nanoparticles on a Polyethylene Terephthalate Substrate. *J. Mater. Chem.* **2010**, *20*, 907–915.
21. Friend, R. H.; Gymer, R. W.; Holmes, A. B.; Burroughes, J. H.; Marks, R. N.; Taliani, C.; Bradley, D. D. C.; Dos Santos, D. A.; Bredas, J. L.; Logdlund, M.; *et al.* Electroluminescence in Conjugated Polymers. *Nature* **1999**, *397*, 121–128.
22. Roberts, M. E.; Mannsfeld, S. C. B.; Stoltenberg, R. M.; Bao, Z. Flexible, Plastic Transistor-Based Chemical Sensors. *Org. Electron.* **2009**, *10*, 377–383.
23. Torsi, L.; Dodabalapur, A. Organic Thin-Film Transistors as Plastic Analytical Sensors. *Anal. Chem.* **2005**, *77*, 380A–387A.
24. Petropoulos, A.; Goustouridis, D.; Speliotes, T.; Kaltsas, G. Demonstration of a New Technology Which Allows Direct Sensor Integration on Flexible Substrates. *Eur. Phys. J. Appl. Phys.* **2009**, *46*, 12507.
25. Liao, F.; Chen, C.; Subramanian, V. Organic TFTs as Gas Sensors for Electronic Nose Applications. *Sens. Actuators, B* **2005**, *107*, 849–855.

26. Kim, Y. S. Microheater-Integrated Single Gas Sensor Array Chip Fabricated on Flexible Polyimide. *Sens. Actuators, B* **2006**, *114*, 410–417.
27. Mabrook, M. F.; Pearson, C.; Petty, M. C. Inkjet-Printed Polypyrrole Thin Films for Vapour Sensing. *Sens. Actuators, B* **2006**, *115*, 547–551.
28. Saran, N.; Parikh, K.; Suh, D. S.; Munoz, E.; Kolla, H.; Manohar, S. K. Fabrication and Characterization of Thin Films of Single-Walled Carbon Nanotube Bundles on Flexible Plastic Substrates. *J. Am. Chem. Soc.* **2004**, *126*, 4462–4463.
29. Li, B.; Santhanam, S.; Schultz, L.; Jeffries-El, M.; Iovu, M. C.; Sauve, G.; Cooper, J.; Zhang, R.; Revelli, J. C.; Kusne, A. G.; *et al.* Inkjet Printed Chemical Sensor Array Based on Polythiophene Conductive Polymers. *Sens. Actuators, B* **2007**, *123*, 651–660.
30. Lee, C.-Y.; Wu, G.-W.; Hsieh, W.-J. Fabrication of Micro Sensors on a Flexible Substrate. *Sens. Actuators, A* **2008**, *147*, 173–176.
31. Su, P.-G.; Wang, C.-S. Novel Flexible Resistive-Type Humidity Sensor. *Sens. Actuators, B* **2007**, *123*, 1071–1076.
32. Sun, Y.; Wang, H. H. Electrodeposition of Pd Nanoparticles on Single-Walled Carbon Nanotubes for Flexible Hydrogen Sensors. *Appl. Phys. Lett.* **2007**, *90*, 213107.
33. McAlpine, M. C.; Ahmad, H.; Wang, D.; Heath, J. R. Highly Ordered Nanowire Arrays on Plastic Substrates for Ultrasensitive Flexible Chemical Sensors. *Nat. Mater.* **2007**, *6*, 379–384.
34. Sayago, I.; Terrado, E.; Aleixandre, M.; Horrillo, M. C.; Fernández, M. J.; Lozano, J.; Lafuente, E.; Maser, W. K.; Benito, A. M.; Martinez, M. T.; *et al.* Novel Selective Sensors Based on Carbon Nanotube Films for Hydrogen Detection. *Sens. Actuators, B* **2007**, *122*, 75–80.
35. Cattanach, K.; Kulkarni, R. D.; Kozlov, M.; Manohar, S. K. Flexible Carbon Nanotube Sensors for Nerve Agent Simulants. *Nanotechnology* **2006**, *17*, 4123–4128.
36. Fu, D.; Lim, H.; Shi, Y.; Dong, X.; Mhaisalkar, S. G.; Chen, Y.; Moochhala, S.; Li, L. Differentiation of Gas Molecules Using Flexible and All-Carbon Nanotube Devices. *J. Phys. Chem. C* **2008**, *112*, 650–653.
37. Marinov, V. R.; Atanasov, Y. A.; Khan, A.; Vaselaar, D.; Halvorsen, A.; Schulz, D. L.; Chrisey, D. B. Direct-Write Vapor Sensors on FR4 Plastic Substrates. *IEEE Sens. J.* **2007**, *7*, 937–944.
38. Joseph, Y.; Peić, A.; Chen, X.; Michl, J.; Vossmeyer, T.; Yasuda, A. Vapor Sensitivity of Networked Gold Nanoparticle Chemiresistors: Importance of Flexibility and Resistivity of the Interlinkage. *J. Phys. Chem. C* **2007**, *111*, 12855–12859.
39. Briseno, A. L.; Tseng, R. J.; Ling, M. M.; Falcao, E. H. L.; Yang, Y.; Wudl, F.; Bao, Z. N. High-Performance Organic Single-Crystal Transistors on Flexible Substrates. *Adv. Mater.* **2006**, *18*, 2320–2324.
40. Chen, F. C.; Chen, T. D.; Zeng, B. R.; Chung, Y. W. Influence of Mechanical Strain on the Electrical Properties of Flexible Organic Thin-Film Transistors. *Semicond. Sci. Technol.* **2011**, *26*, 034005.
41. Verma, V. P.; Das, S.; Lahiri, I.; Choi, W. Large-Area Graphene on Polymer Film for Flexible and Transparent Anode in Field Emission Device. *Appl. Phys. Lett.* **2010**, *96*, 203108.
42. Herrmann, J.; Muller, K. H.; Reda, T.; Baxter, G. R.; Raguse, B.; de Groot, G. J. J. B.; Chai, R.; Roberts, M.; Wieczorek, L. Nanoparticle Films as Sensitive Strain Gauges. *Appl. Phys. Lett.* **2007**, *91*, 183105.
43. Brust, M.; Walker, M.; Bethell, D.; Schiffrin, D. J.; Whyman, R. Synthesis of Thiol-Derivatised Gold Nanoparticles in a Two-Phase Liquid–Liquid System. *J. Chem. Soc., Chem. Commun.* **1994**, 801–802.
44. Hostetler, M. J.; Wingate, J. E.; Zhong, C. J.; Harris, J. E.; Vachet, R. W.; Clark, M. R.; Londono, J. D.; Green, S. J.; Stokes, J. J.; Wignall, G. D.; *et al.* Alkanethiolate Gold Cluster Monolayers with Radii from 7 to 26 Angstroms: Borders between Molecular and Metallic Behavior and between Two- and Three-Dimensional Monolayers. *Langmuir* **1998**, *14*, 17–30.